A Robust Molecular Catalyst Generated In Situ for Photo- and Electrochemical Water Oxidation

Hussein A. Younus,[a, b, c, g] Nazir Ahmad,[a, b, c] Adeel H. Chughtai,[a] Matthias Vandichel,[e, f] Michael Busch,[f] Kristof Van Hecke,[d] Mekhman Yusubov,[c] Shaoxian Song,[b] and Francis Verpoort*[a, b, c, d]

Water splitting is the key step towards artificial photosystems for solar energy conversion and storage in the form of chemical bonding. The oxidation of water is the bottle-neck of this process that hampers its practical utility; hence, efficient, robust, and easy to make catalytic systems based on cheap and earth-abundant materials are of exceptional importance. Herein, an in situ generated cobalt catalyst, $[Co^{II}(TCA)_2(H_2O)_2]$ (TCA = 1-mesityl-1,2,3-1H-triazole-4-carboxylate), that efficiently conducts photochemical water oxidation under near-neutral conditions is presented. The catalyst showed high stability under photolytic conditions for more than 3 h of photoirradiation. During electrochemical water oxidation, the catalytic system assembled a catalyst film, which proved not to be cobalt oxide/hydroxide as normally expected, but instead, and for the first time, generated a molecular cobalt complex that incorporated the organic ligand bound to cobalt ions. The catalyst film exhibited a low overpotential for electrocatalytic water oxidation (360 mV) and high oxygen evolution peak current densities of 9 and 2.7 mA cm^{-2} on glassy carbon and indium-doped tin oxide electrodes, respectively, at only 1.49 and 1.39 V (versus a normal hydrogen electrode), respectively, under neutral conditions. This finding, exemplified on the in situ generated cobalt complex, might be applicable to other molecular systems and suggests that the formation of a catalytic film in electrochemical water oxidation experiments is not always an indication of catalyst decomposition and the formation of nanoparticles.

Introduction

Nature, represented in plants and a few microorganisms, has provided an extraordinary way to utilize solar energy for making life on our planet and given us an ideal blueprint to mimic their comportment. Inspired by the natural oxygen-evolving complex (OEC) in photosystem II,[1] remarkable efforts have been devoted towards the development of single-site and multinuclear transition-metal (TM) complexes that enable water oxidation (WO) for artificial photosynthesis.[2] Several molecular catalytic systems for WO have been developed based on ruthenium,[3] iridium,[4] cobalt,[5] copper,[6] manganese,[7] iron,[8] and nickel.[9] Moreover, tremendous efforts have been devoted to materials based on TM oxides and hydroxides.[10] Because of cost considerations, the development of highly active catalysts for WO based on earth-abundant TMs is essential for practical applications and would greatly enhance the commercial viability of solar energy.[8b, 11] Although cobalt is significantly less abundant (20–30 ppm) than iron (6.3%), manganese (0.1%), nickel (90 ppm), or copper (68 ppm) in the outer layer of the earth's crust, it is now the most researched metal for its catalytic power in both WO and hydrogen evolution.[12] Catalyst robustness, effectiveness, and benign operating conditions (such as neutral pH, low-to-moderate overpotential, and

[a] Dr. H. A. Younus, Dr. N. Ahmad, Dr. A. H. Chughtai, Prof. F. Verpoort
State Key Laboratory of Advanced Technology for Materials
Synthesis and Processing, Wuhan University of Technology
Wuhan 430070 (P.R. China)
E-mail: francis.verpoort@ugent.be

[b] Dr. H. A. Younus, Dr. N. Ahmad, Prof. S. Song, Prof. F. Verpoort
School of Resources and Environmental Engineering
Wuhan University of Technology
Wuhan 430070 (P.R. China)
E-mail: francis.verpoort@ugent.be

[c] Dr. H. A. Younus, Dr. N. Ahmad, Prof. M. Yusubov, Prof. F. Verpoort
National Research Tomsk Polytechnic University
Lenin Avenue 30, Tomsk 634050 (Russia)
E-mail: francis.verpoort@ugent.be

[d] Prof. K. Van Hecke, Prof. F. Verpoort
Department of Inorganic and Physical Chemistry
Laboratory of Organometallic Chemistry and Catalysis

Ghent University, Krijgslaan 281 (S-3)
9000 Ghent (Belgium)
E-mail: francis.verpoort@ugent.be

[e] Dr. M. Vandichel
Center for Molecular Modeling, Ghent University
Technology Park 903, 9052 Zwijnaarde (Belgium)

[f] Dr. M. Vandichel, Dr. M. Busch
Department of Physics and Competence Center for Catalysis
Chalmers University of Technology
Fysikgränd 3, Göteborg (Sweden)

[g] Dr. H. A. Younus
Chemistry Department, Faculty of Science
Fayoum University
Fayoum, 36514 (Egypt)

Supporting Information and the ORCID identification number(s) for the author(s) of this article can be found under http://dx.doi.org/10.1002/cssc.201601477.

temperature) make cobalt-based catalysts the most promising candidates for both WO and reduction.[12a]

Molecular catalytic systems are recognized for their tunable redox properties and facile characterization of their active intermediates, which are necessary for related mechanistic studies. However, the identity of the active catalyst must be investigated in depth before a detailed interrogation of the water oxidation catalyst (WOC) mechanism. The identification of the real catalyst is extremely challenging, especially in studies on cobalt-based homogeneous WOCs.[5b, 13] This is mainly because small amounts of cobalt oxide may be produced from the decomposition of the molecular catalyst that work as an efficient catalyst during the WO reaction.[13b, 14] Indeed, some catalysts thought to be the real WOCs have subsequently been demonstrated to act as precursors of heterogeneous materials, which are the active catalysts.[13b, 15] In other cases, cubane Co_4O_4 clusters in $Co_4O_4(Ac)_4(py)_4$ (py = pyridine) were primarily introduced as homogeneous WOCs, but recently it was confirmed that the observed WO activity originated from Co^{II} impurities rather than the Co_4O_4 clusters.[16] Nonetheless, there are also examples of cobalt complexes that do function as homogeneous, molecular WOCs.[11b, 17]

All cobalt WOCs reported so far, in both homo- and heterogeneous systems, are mainly based on polydentate ligands, which are likely to be necessary for stabilizing cobalt ions in higher oxidation states. In most cases, the ligand is rigid, which might prevent the complex from any expected conformational changes during the catalytic mechanism to finally deliver oxygen. Additionally, most of the reported homogenous molecular cobalt complexes, if not all, are based on tetra- or pentadentate ligands that require a special design and may not be easy to tune or even synthesize. This inspired us to explore cobalt complexes based on a bidentate ligand to see whether the polydentate ligand nature was crucial to maintain the homogeneity of the catalytic system or not. Moreover, the strong influence of an anionic carboxylate ligand on ruthenium WOCs proved to be very effective at stabilizing higher oxidation states, resulting in unprecedentedly high reaction rates with a turnover frequency comparable to the rate of the OEC of the natural photosystem.[18]

Herein, we present the in situ generated mononuclear cobalt(II) complex $[Co(TCA)_2(H_2O)_2]$ (**1**; TCA = 1-mesityl-1,2,3-1H-triazole-4-carboxylate) as a molecular catalyst for both electro- and photochemical WO. The catalyst was prepared in situ from commercially available cobalt acetate and 1-aryl-1H-1,2,3-triazole-4-carboxylic acid in an acetate buffer solution under near-neutral conditions (pH 6–7). Several lines of evidence, such as those obtained by dynamic light scattering (DLS), ESI-MS, ^{1}H NMR spectroscopy, and FTIR spectroscopy, demonstrate that the system works as a molecular catalyst under visible-light irradiation, with $[Ru(bpy)_3]^{2+}$ (bpy = 2,2′-bipyridine) as a photosensitizer (PS) and persulfate as a sacrificial electron acceptor. Moreover, the catalytic system generates a catalytic active film on a glassy carbon electrode (GCE) that is highly efficient for electrocatalytic WO. The current density reaches about 9 mA cm^{-2} at only 1.49 V (versus a normal hydrogen electrode (NHE)) at pH 6 ($\approx$600 mV overpotential). Several

characterization techniques, including SEM, energy-dispersive X-ray spectroscopy (EDX), X-ray photoelectron spectroscopy (XPS), and Raman spectroscopy, of the deposited film on both glassy carbon (GC) and indium-doped tin oxide (ITO) electrodes revealed that brown film deposition is not indicative of cobalt oxide nanoparticle formation during electrochemical WO, as normally expected, but might be a result of the formation of a molecular species incorporating the organic ligand bound to the cobalt ions. More interestingly, the deposited brown film could be dissolved in organic solvents, such methanol and chloroform, which enabled its further characterization by ^{1}H NMR and FTIR spectroscopy; these results matched completely with the isolated product after photochemical WO experiments.

Results and Discussion

Synthesis and characterization

Ligand design and consequently catalyst optimization are influential for O_2 production and many multi-coordinating ligands are accessible to produce new catalytic systems. To develop a low-cost and viable catalyst for the WO reaction, we took care to use earth-abundant metal cobalt complexes that could be prepared in an aqueous medium upon direct mixing from easily accessible sources. The straightforward construction of a triazole ring, along with possible immobilization on any azide- or alkyne-functionalized surface, is also very attractive for using a substituted triazole ring as a bidentate ligand for WO.[19] The bidentate ligand, 1-aryl-1H-1,2,3-triazole-4-carboxylic acid, was readily prepared through the copper-catalyzed azide–alkyne cycloaddition click reaction of aryl azide and propiolic acid. Then, the catalyst was prepared by adding cobalt acetate to a predissolved ligand in acetate buffer (Scheme 1). In situ catalyst formation was established based on UV/Vis spectroscopy and ESI-MS results, and also confirmed in the solid state from X-ray single-crystal analysis.

In the UV/Vis absorption spectra of TCA ligand, there are two weak absorption bands with maxima at $\lambda = 269$ and 274 nm, in both MeOH and acetate buffer (pH 6; Figure S1 in the Supporting Information), whereas cobalt acetate has an absorption band at $\lambda = 519$ nm. Mixing ligand and cobalt acetate in a 2:1 ratio in buffer directly resulted in complete disappearance of the band corresponding to cobalt acetate and the appearance of a new broad band from $\lambda = 580$ to 400 nm with a maximum at $\lambda = 483$ nm (Figure S2). The new band did not differ over time after several scans at different intervals and was in excellent agreement with the band of the as-synthesized complex. The use of different ratios of ligand to cobalt ions did not lead to any differences in the UV/Vis spectra of the complexes (Figure S3). The colors of the different in situ generated complexes in acetate buffer are identical, except in the case of a 1:1 ratio; the color remained light pink and was derived from the cobalt acetate source. This can be interpreted as the result of two ligands coordinating to one cobalt ion and the coexistence of free cobalt ions. This point was also confirmed by isolating the same product with different ligand-to-
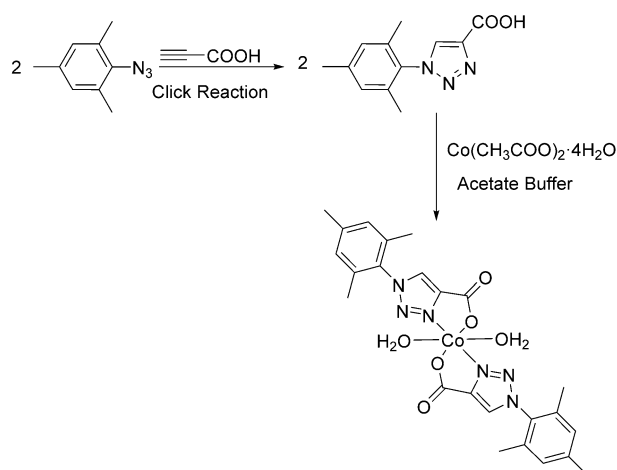
Scheme 1. Synthesis of [Co(TCA)$_2$·2H$_2$O] (1).

Figure 1. Thermal ellipsoid plot of 1 (at the 50% probability level).

metal ratios, as indicated by solid-state X-ray single-crystal analysis. UV/Vis spectroscopy did not show a clear difference in case of a 1:1 ratio owing to the low molar absorptivity of cobalt acetate. Trials to follow complex formation under the same conditions (in acetate buffer prepared in D$_2$O) failed owing to the instant precipitation of the complex at the higher concentrations used for NMR sampling.

Slow evaporation of an aqueous solution of complex (5 mM) in acetate buffer results in light brown crystals within two days. The ESI-MS spectrum of the separated catalyst crystals exposed a strong signal at m/z 553.42, corresponding to [Co(TCA)$_2$(H$_2$O)$_2$] [$M^+ - 2H^+$]. Interestingly, crystals suitable for X-ray crystallography were obtained from low-concentration solutions (1 mM) within three to four weeks from acetate buffer (pH 6); this supports the notion that the complex structure is highly robust in buffer solution for a long time. Compound 1 crystallized in the centrosymmetric triclinic space group P$\bar{1}$. As it is clear from this space group, the inverted structure or mirror image is present in the crystal for 50% of the unit cells, but the asymmetric unit contains two halves of crystallographically independent, isostructural Co(TCA)$_2$(H$_2$O)$_2$ complexes, with both Co^{II} ions located on inversion centers, together with two solvent water molecules. Hence, a complete Co(TCA)$_2$(H$_2$O)$_2$ complex is built up by an inversion center itself. As a consequence, this means that the inverted structures of the first Co(TCA)$_2$(H$_2$O)$_2$ complex, as well as that of the second complex, are exactly the same and can be perfectly superposed on each other, preserving the configuration (see Figure S5). Therefore, it is not likely that induced chirality might influence the efficiency of catalysis. Each cobalt center exhibits an octahedral coordination geometry, that is, two TCA ligands bidentately coordinate through both nitrogen and carboxylate oxygen donor atoms, forming the octahedron equatorial plane, along with two aqua ligands, occupying the axial positions (Figure 1). The Co—O and Co—N distances range from 2.070(3) to 2.124(3) Å and 2.115(3) to 2.138(3) Å, respectively. In the crystal packing, π–π stacking interactions are observed between the aromatic triazole and mesityl rings (centroid–centroid distances in the range of 5.053(2)–5.948(2) Å). CH–π inter-

actions are observed between mesityl rings (C–centroid distances between 3.798(5) and 3.893(5) Å). The two cobalt centers prominently feature the presence of an exchangeable two aqua-coordination site on each of cobalt(II) ions. Most likely, the use of the flexible bidentate coordinating ligands allow the ligand to remain constantly coordinated to the metal center within the complete catalytic cycle. Another feature of the catalyst structure is the sheet-like hydrogen-bond network in the (010) plane, which interlocks the oxo bridges, coordinated water, and solvent water molecules (Figure S6).
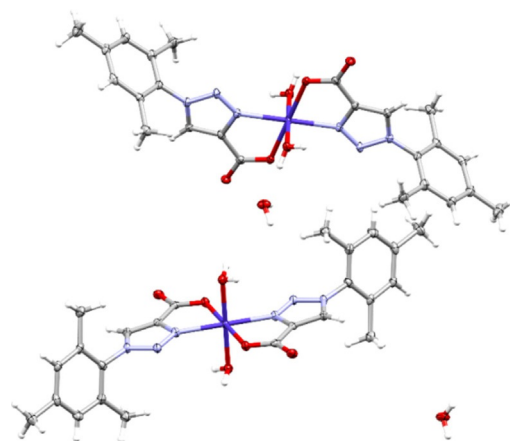
Electrocatalytic investigations

We started our study by investigating the electrochemical properties of cobalt acetate in acetate buffer (pH 6.0–6.03). A 1 mM solution of cobalt acetate showed an irreversible current wave with an onset potential of about 1.15 V versus Ag/AgCl (all potentials presented herein are referenced to the Ag/AgCl electrode). The current reaches about 125 µA at 1.3 V in the first scan, with no substantial increase in the catalytic current with the next 100 cyclic voltammetry (CV) scans in the range 0–1.3 V (Figure 2A). LSV with a fresh GCE exhibited a relatively high catalytic current of about 192 µA at 1.3 V and the catalytic oxidation wave did not show significant changes after 100 scans (Figure 2B). The SEM topography of the electrode-posited materials on the GCE surface showed the formation of an amorphous powder similar to material, which proved to be cobalt oxide, reported recently in case of using an ITO electrode (Figure S7).[20] Nevertheless, based on LSV data, monitored after using the GCE for several CV scans, the growth of these materials was very slow. EDX analysis enabled the determination of the elemental composition of the deposited material (Figure S7). Data confirm the presence of cobalt, sodium, and oxygen. The oxygen to cobalt ratio in the deposited material is consistent with the formation of an oxide/hydroxide film. Moreover, when the GCE was removed from the catalyst solution after 100 CV scans, thoroughly rinsed with water, and then placed into cobalt-free acetate buffer solution, nearly the same catalytic current was observed as that when the electrode was used in the presence of cobalt acetate. This behavior
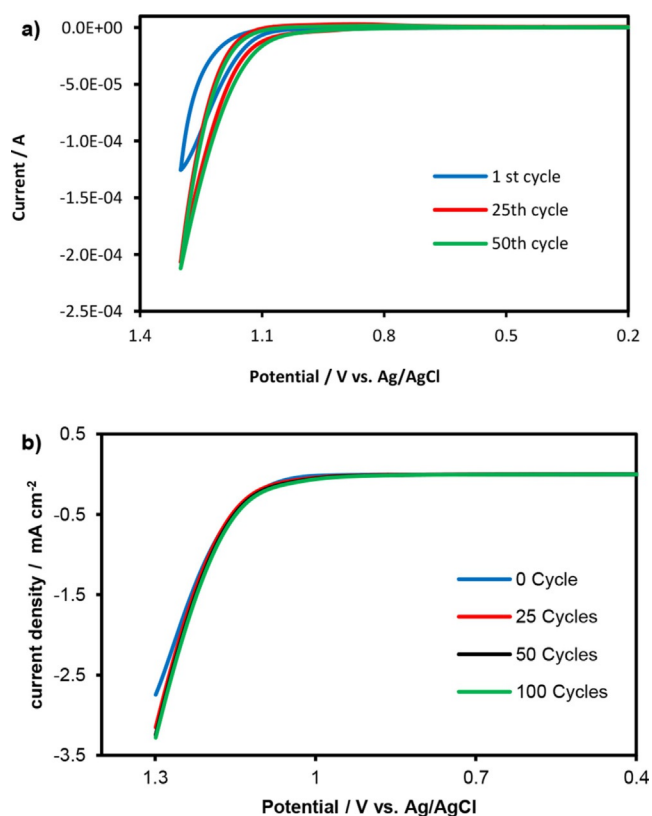
Figure 2. a) Cyclic voltammogram of 1 mM cobalt acetate in 0.1 M sodium acetate (pH 6) at a scan rate of 50 mV s^{-1} with a 3 mm GC working electrode, platinum wire as a counter electrode, and a Ag/AgCl (with a 3 M aqueous solution of KCl) reference electrode. b) Linear sweep voltammetry (LSV) of 1 mM cobalt acetate in 0.1 M sodium acetate (pH 6); scans were taken by using a fresh GCE (blue) and a previously used electrode for several consecutive CV scans, 25 (red), 50 (black), and 100 cycles (green), in the range 0–1.3 V. The scan rate was 50 mV s^{-1}.

supports the hypothesis of cobalt oxide/hydroxide film formation on the surface of the GCE.

The addition of TCA ligand in a 2:1 ratio to cobalt ions resulted in a significant change in the electrochemical properties. Two equivalents of the ligand were dissolved in 0.1 M acetate buffer, followed by the addition of one equivalent of cobalt acetate. Directly after mixing, the cyclic voltammograms of the Co–2TCA system showed an irreversible oxidation peak with an initial current of about 121 µA at 1.3 V (versus Ag/AgCl electrode; Figure 3 A). As shown in the cyclic voltammograms, after 100 scans, the catalytic current increases about fourfold, which suggests the formation of a catalyst film on the electrode surface. After 100 CV scans, the current reached a measured value of 403 µA at 1.30 V, corresponding to a current density of 5.75 mA cm^{-2} (at pH 6); the onset potential also reached a value of 1.03 V (corresponding to an overpotential of 360 mV). This current density is much higher than those reported recently for a cobalt(II)-based catalyst for WO deposited on fluorine-doped tin oxide (FTO) electrodes, showing a current density of < 1 mA cm^{-2} at 1.5 V (versus Ag/AgCl) in pH 7 phosphate buffer, at the same scan rate (50 mV s^{-1}).[21] In addition, it is favorable to compare our system with other excellent WOCs reported previously. For example, a highly efficient cobalt car-
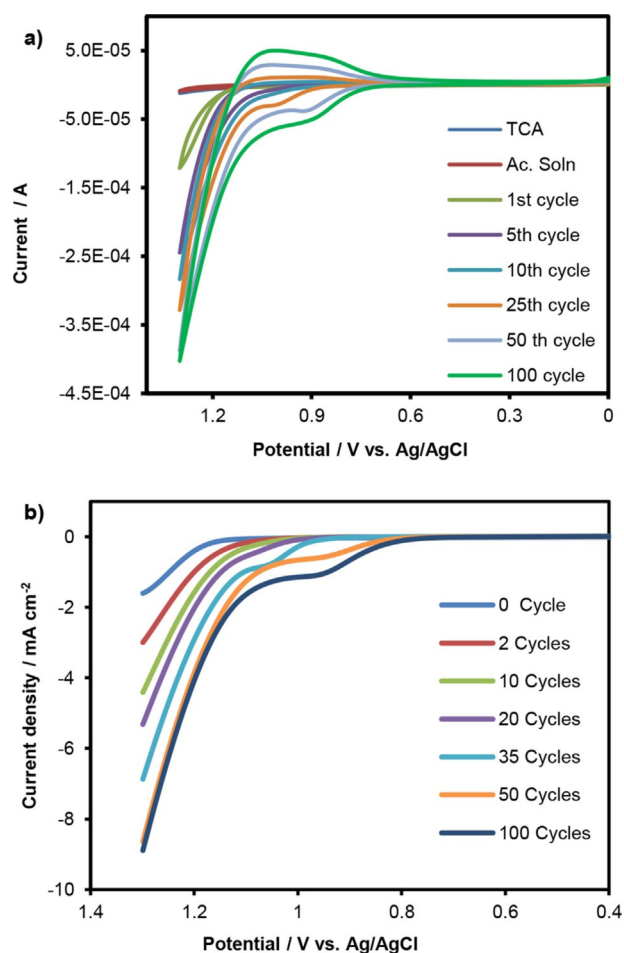
Figure 3. Electrochemical response of Co–2TCA under different experimental conditions. a) 100 consecutive CV scans were performed on an aqueous 1 mM solution of Co–2TCA in 0.1 M acetate buffer, pH 6, scan rate = 50 mV s^{-1}; 1 (blue), 5 (green), 10 (red), 25 (pink), 50 (brown), and 100 cycles (black). b) LSV results for 1 mM Co–2TCA in 0.1 M sodium acetate (pH 6); scans were taken by using a fresh GCE (blue) and a previously used electrode for 5 (brown), 25 (green), 50 (pink), and 100 consecutive CV scans (black), in the range 0–1.3 V.

bonate (Co–Ci) film generated from cobalt(II) in neutral bicarbonate buffer showed a current density of 4.1 mA cm^{-2} with a GCE at 1.3 V (versus Ag/AgCl), at pH 7.[22] To check any possibility of ligand oxidation under the operating conditions, CV in the absence of cobalt acetate with the TCA ligand only in acetate buffer (pH 6) showed only double-layer charging currents, with no significant Faradaic component (Figure 3 A). In some other cases in which mononuclear cobalt complexes with organic ligands decomposed to give nanoparticles in the photocatalytic WO systems, the organic ligand suffered electrochemical oxidation at a potential lower than 1.0 V (versus a saturated calomel electrode (SCE)) under similar operating conditions.[23]

LSV was used to confirm the catalyst film growth by screening the catalytic current after several successive CV scans. For a freshly polished GCE, LSV showed an oxidative wave with an onset potential of about 1.1 V (versus Ag/AgCl) and a wave catalytic current of 106 µA at 1.3 V. As the number of CV scans increases, the oxidation wave increases fivefold in magnitude

and shifts to lower onset potentials after the first 100 CV scans (Figure 3 B). Because the catalytic oxidation wave increases over time, the initial catalyst cannot be the most active catalyst and may be converted into another more active form. An equilibrium between monomer diaqua cobalt complex **1** and oligo-/polymer or other molecular species that can be generated under the external potential can account for film formation. Moreover, the current crossover observed in the first cycle of CV at the onset potential, at which the catalytic wave of the anodic scan showed a higher current than that of the reverse scan, presumably owing to the resolution of the deposited film.

Several obtained data support the point that the deposited film from the Co−2TCA catalytic system is a molecular cobalt species rather than oxide/hydroxide film formation. The in situ generated complex maintains a high hydrolytic stability and solubility (with concentrations up to 2 mM) in acetate solution (pH 6–8), as confirmed by UV/Vis spectroscopy and electrochemical measurements. UV/Vis spectroscopy did not show any change for a solution of catalyst in acetate aged for one month compared with that of a freshly mixed one. LSV results for a freshly mixed and one-month aged solution were also identical. This confirms that the most active form of the catalyst is formed upon applying the potential and not because of decomposition of the complex under operating conditions, such as pH or aqueous hydrolysis. This is different from some other catalytic systems based on cobalt polyoxometalates, for which nanoparticles formed directly after dissolution in buffer solutions.[13b] After 100 CV scans, the electrode was removed from the catalyst solution and rinsed thoroughly with deionized water. CV in catalyst-free acetate buffer shows a clear drop in the catalytic current. This can be interpreted as follows: Initially, a film is formed on the electrode surface with continuous scanning owing to an equilibrium between solution and surface species. Then, in catalyst-free acetate buffer, this equilibrium is subjected to change and the film redissolves in the buffer solution, resulting in a clear drop in the catalytic current after several CV scans, as shown in Figure S8 A.[24] Thereafter, under the same conditions, LSV revealed a decrease in the magnitude of the catalytic current by about fivefold and shifted to a higher onset potential (Figure S8 B). In the case of cobalt acetate, a rinsed electrode in buffer alone shows the same features as those seen in the solution of cobalt acetate; however, no signals are present after polishing.

By using a highly oriented pyrolytic graphite (HOPG) electrode (basal plane), the in situ generated complex shows different electrochemical features. Cyclic voltammograms showed a quasi-reversible oxidation wave at 0.75 V that was assigned to Co[III/II] oxidation and an irreversible catalytic wave with an onset potential of about 1.05 V, which reached an initial current of about 161 μA at 1.3 V (versus Ag/AgCl electrode; Figure 4 A). In DPV, the peak of Co[III/II] appears clearly at 0.668 V (Figure 4 B). Remarkably, catalytic film electrodeposition on the HOPG electrode was slower than that on a GCE because the wave current was amplified by 50 % after 25 CV cycles compared with 250 % in case of GCE. This catalytic current of the HOPG film declined within 20 CV scans when used in catalyst-
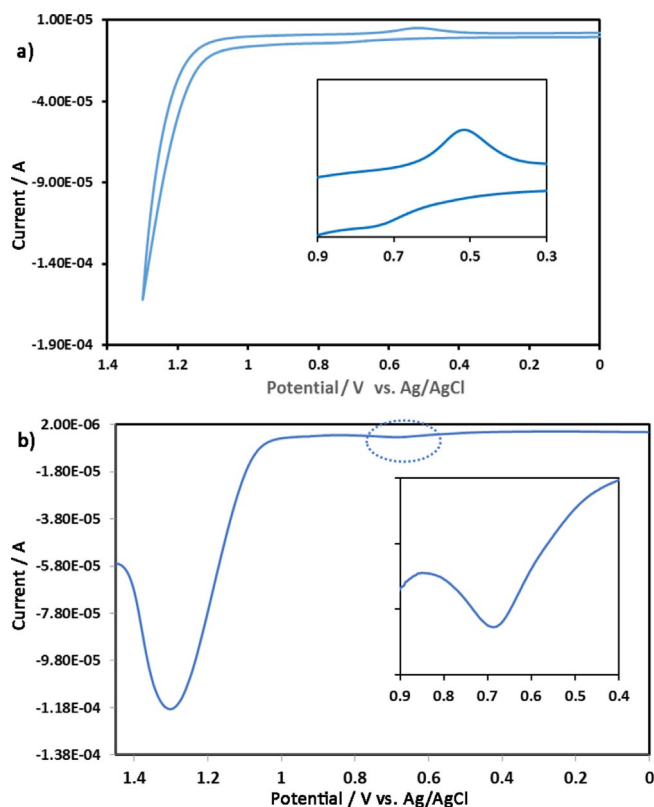
Figure 4. CV (A) and differential pulse voltammetry (DPV; B) electrochemical responses of a 1 mM solution of Co−2TCA in 0.1 M acetate buffer, pH 6, with a HOPG electrode (basal plane), scan rate = 50 mV s^{−1}.

free acetate buffer owing to film dissolution in the aqueous medium (Figure S9).

To obtain a more comprehensive insight into the electrochemical behavior of the catalytic system, the dependence of the onset potentials on pH was investigated in the pH range of 4.5–9.0. In the pH range 5.5–7.0, the onset of catalysis is shifted to higher potentials as the pH is lowered. The onset potential versus pH plot shows typical Nernstian behavior with 60 mV per pH shift, revealing that one-electron oxidation is accompanied by the transfer of one proton (proton-coupled electron transfer (PCET)), which is ascribed to the $[Co^{IV}=O]/[Co^{III}-OH]$ redox couple. At higher pH values ($7.0 < pH \leq 8.7$), the oxygen onset potential remains constant. This is in contrast with the shift of approximately 60 mV per pH unit for the oxygen onset potential, which means that the electron transfer step is not coupled to proton transfer.[25] At pH > 9, the onset potential shifts to higher values and the catalytic current for the WO reaction decreases to more than 65 % of its value at pH 8.7; this is a result of the decomposition of the catalyst under these basic conditions and the formation of cobalt hydroxide precipitate (Figure S10). Below pH 5.5, a large positive shift in the onset potential and diminished current density is observed.

An initial investigation of the deposited catalyst film on the GCE surface after 100 CV cycles by means of Raman spectroscopy showed two strong bands at 2654 and 2910 cm^{−1}, and another weak band at 3239 cm^{−1} (Figure 5). These bands corre-
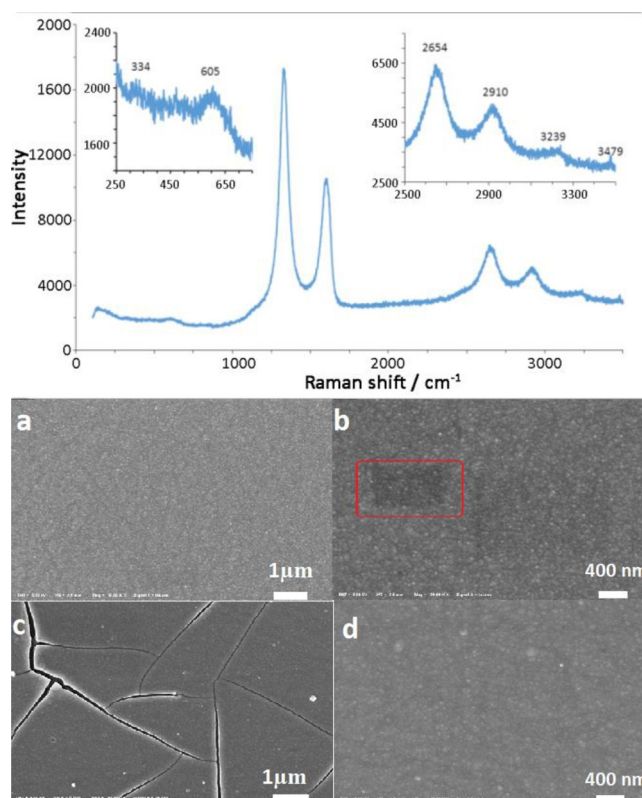
Figure 5. Raman spectrum (top) and field-emission (FE) SEM images of the deposited film on a GCE (bottom); after 100 CV scans in the range 0–1.3 V versus Ag/AgCl electrode with a scan rate of 50 mV s^{-1} (a, b), and after 1 h of electrolysis (c, d) at 1.2 V versus Ag/AgCl electrode, of an aqueous 1 mM solution of Co−2 TCA in 0.1 M acetate buffer (pH 6).

spond to C−H aliphatic/aromatic stretching vibrations that cannot arise from the cobalt oxide film. Interestingly, the band at 3479 cm^{-1} fits with the O−H stretching vibration of the cobalt-coordinated aqua ligand. The relatively low feature observed in the range 544–712 cm^{-1} for the Co−O bond is what would have been expected if Co were present as a metal–organic film rather than as cobalt oxide.[26] Moreover, the weak band in the range 302–575 cm^{-1} can be ascribed to the Co−N bond from the metal complex.[27]

SEM images of the electrodeposited catalytic film on a GCE showed complete coverage of the electrode surface, with a uniform film distribution across the surface. Notably, the high-energy ($\approx$15 keV) incident electron beam resulted in burning of the deposited film, which indicated the organometallic nature of the film (Figure 5). EDX revealed that the deposited catalytic film contained Co, O, and C with an approximate Co/O ratio of 1:2.59. This high oxygen to cobalt ratio cannot be justified based on cobalt oxide structures, such as CoO or Co$_3$O$_4$, in which the oxygen content is lower than that of cobalt. In a molecular film of the complex, the Co/O ratio is calculated to be 1:2, which is closer to the observed value. Moreover, the absence of any traces of sodium ions from the buffer solution in the deposited film strongly supports the molecular identity of the film. In contrast, for cobalt oxide catalyst films, cations from the buffer solution, typically sodium and potassium, are commonly observed in the film struc-

ture.[13b, 20, 28] The low ratio of nitrogen content detected by EDX might be attributed to the low sensitivity of this method to the surface composition (Figure S11).[29] EDX results of the deposited film in the case of the ITO electrode gave evidence of carbon incorporation into the catalyst film.

For further characterization and to confirm the molecular identity of the deposited catalytic active film, we used an ITO electrode with a larger surface area (0.5 cm^2) in a controlled potential electrolysis experiment. After 11 h of electrolysis at 1.2 V (versus Ag/AgCl), a transparent brownish film about 400 nm thick was formed on the ITO electrode (Figure 6). The elemental composition of the post-electrolysis ITO electrode and the valence states of metal elements were studied by means of XPS. The XPS survey spectra recorded for the catalyst film indicated the presence of N 1s, C 1s, O 1s, and Co 2p peaks, along with In and Sn from the electrode surface (Figure 6). The HR-XPS spectrum of cobalt showed two major peaks at 780.9 and 796.5 eV, corresponding to Co 2p$_{3/2}$ and Co 2p$_{1/2}$, respectively. The absence of broad satellites (shake-up peaks), along with Co 2p$_{1/2}$–2p$_{3/2}$ spin–orbit level energy spacing ($\approx$15.5 eV), supports the presence of low-spin Co^{III}.[30] XPS signals at 60 and 102 eV are also consistent with the presence of Co 3s and Co 3p.

The C 1s core-level spectrum displayed several peaks owing to different functionalized carbon atoms. The spectrum suggests the presence of C=C, C−C, C−N, and COO in the deposited film, as observed in the peaks at 284.5, 285.2, 286.6, and 288.5 eV, respectively. Remarkably, no C 1s peak corresponding to carboxylic carbon (−COOH) appeared in the spectrum, which indicated the absence of free ligand.[31] This rules out ligand codeposition with a metal oxide film and confirms ligand coordination to the cobalt ion in the formed catalyst film. This C 1s spectrum differs from the case of using cobalt acetate only in acetate buffer, for which two peaks at 285.1 and 288.3 eV represent ionization of the C 1s core level of the methyl and carboxylate carbon atoms, respectively, from the acetate ion.[20]

The O 1s peaks of Co$_3$O$_4$ and CoO nanoparticles appear in the range of 529.4–530.3 eV.[32] Deconvolution of the O 1s peak gives three contributions at 531.8, 534.5, and 535.5 eV, which are in a higher binding energy region compared with those of lattice oxygen O^{2-} from cobalt oxides. This result clearly shows that no persistent oxide layers are formed at any stage of the catalytic cycle. In addition, based on their binding energy values, these peaks are assigned to O=C, O−C=O, and OH, respectively, from a molecular catalytic film. The N 1s XPS spectrum was deconvoluted into three major components at 399.2, 400.2, and 401.4 eV. The two peaks at high binding energy (400.2 and 401.4 eV) are assigned to free nitrogen atoms from the triazole structure.[33] A change in binding energy of metal-bound nitrogen has been reported in the literature to cause this peak to shift to a lower binding energy of about 399.2 eV.[34] Consequently, the third nitrogen atom from the triazole moiety also preserves its coordination to the cobalt ion in the deposited film.

More very conclusive evidence of the organometallic nature of the formed film was gained by dissolving the film in organic
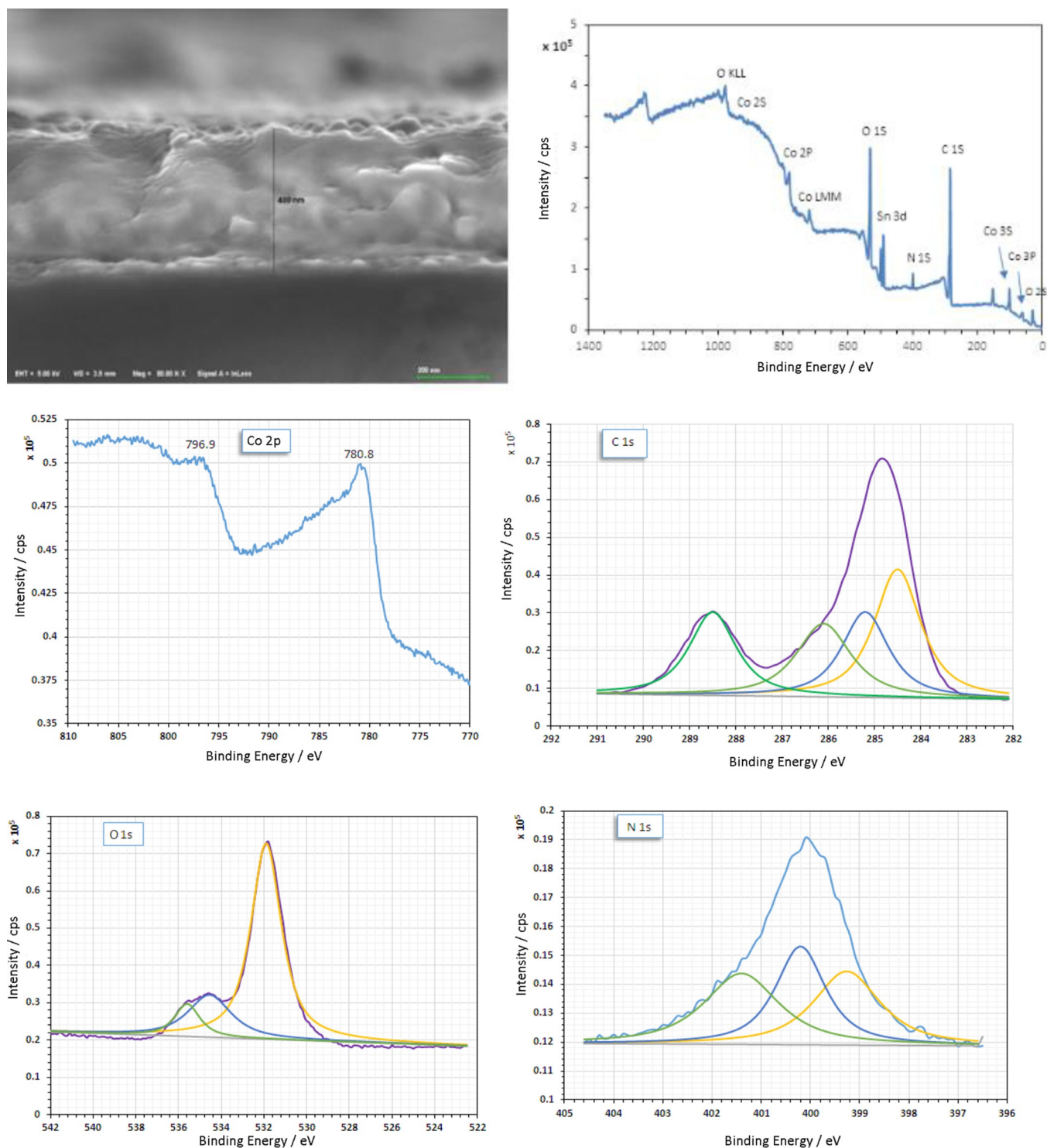
Figure 6. FE-SEM image (top left; scale bar corresponds to 400 nm and the line in the middle to 400 nm), XPS survey spectrum (top right), and high-resolution (HR) scans for Co 2p, C 1s, O 1s, and N 1s regions (bottom) of the deposited film on an ITO electrode after 11 h of CPE at 1.2 V (versus Ag/AgCl), in acetate buffer (pH 6).

solvents. First trials to dissolve the brown film deposited on the ITO electrode in organic solvents, such as chloroform, methanol, ethanol, and acetone, failed. Interestingly, the use of the same deposited catalyst film in complex-free acetate buffer during bulk electrolysis resulted in leaching of the film from the electrode surface into the aqueous solution. This brownish material was soluble in organic solvents, such as chloroform and ethanol. The FTIR spectrum of the film dissolved in chloroform matched well with the isolated product from the photochemical WO experiment, with $[Ru(bpy)_3]^{2+}$ as a PS and persulfate as the sacrificial electron acceptor (as characterized and discussed in detail below) (Figure 7).
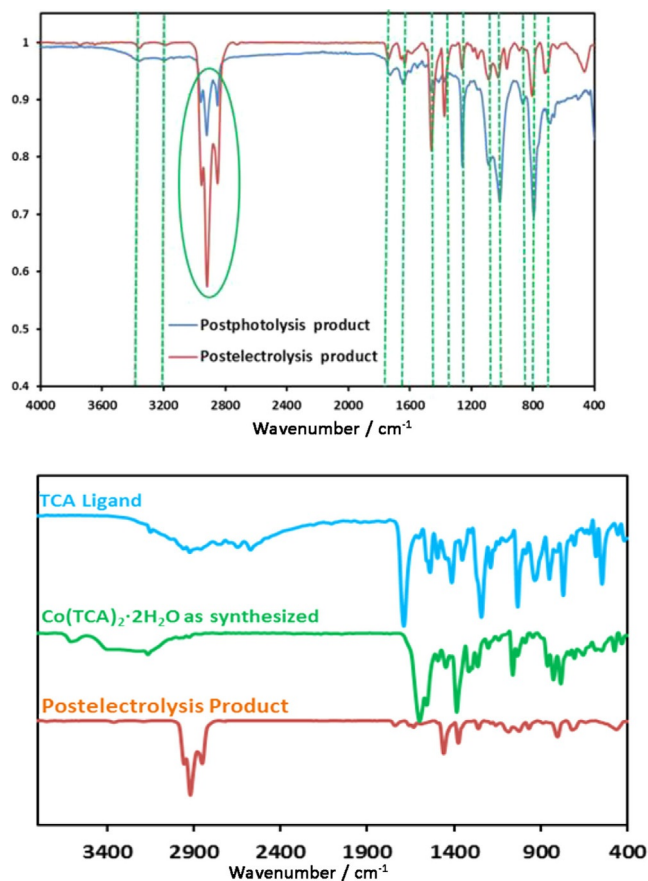
Figure 7. FTIR spectra of the post-electrolysis and post-photocatalysis products (top) and a comparison of the FTIR spectra of the ligand, complex, and post-electrolysis product (bottom).

FTIR spectra of the brown film separated after bulk electrolysis show clear indications of the metal–organic nature of the deposited film. The spectrum of as-synthesized cobalt complex has a broad band in the range of $\tilde{v} = 2880$–3470 cm^{-1} for coordinated water with superimposed weak bands at $\tilde{v} = 2852$, 2918, and 3161 cm^{-1} assigned to C_{sp^3}—H symmetric and asymmetric stretching vibrations and C_{sp^2}—H stretching vibrations, respectively. In addition, there are strong stretching frequencies at $\tilde{v} = 1598$, 1554, 1444, 1384, and 1062 cm^{-1} assigned to $C=O_{str}$, $C=C_{str}$, CH_{3bend}, and C—O_{str} features, respectively. The post-electrolysis/photocatalysis separated brown powder showed a similar pattern to that of the as-synthesized complex with a slight shift in some bands. The aliphatic C—H stretching vibrations, from methyl groups, can be clearly seen as strong bands at $\tilde{v} = 2848$, 2929, and 2952 cm^{-1} together with a weak band at 3200 cm^{-1} owing to aromatic C—H_{sp^2} stretching vibrations. Moreover, there are weak to strong bands at $\tilde{v} = 1635$, 1593, 1460, 1375, 1263, and 1062 cm^{-1} assigned to $C=O_{str}$, $C=C_{str}$, C=N, CH_{3bend}, and C—O_{str} features, respectively. It is worth noting that the broad band in the O—H region of the complex was replaced by a weak, sharp band in the case of the post-electrolysis film.

To further explore the structure of the cobalt species deposited on the working electrode, the brown film formed during

the bulk electrolysis experiment was analyzed by HR-ESI-MS. Analysis of the post-electrolysis film confirmed the existence of complex **1** at m/z 542.10999, which fit well with the calculated value of m/z 542.10889 [$Co(TCA)_2$—H_2O+Na^+]. The same value was observed for the as-synthesized catalyst. However, we could not exclude the formation of some new molecular species because the ESI-MS spectrum of the film exhibited some new signals compared with that of the as-synthesized complex (Figure S12). At the same time, the deposited film was free from any uncoordinated ligand (m/z 231) or cobalt aqua ions [$Co(H_2O)_6$]$^{2+}$ (m/z 167).

Controlled potential electrolysis (CPE) for 11 h in a one-compartment cell with the in situ generated complex did not result in any metal deposition on the counter platinum electrode, whereas in the case of cobalt acetate a black deposition was clearly observed on the counter electrode. Optical spectra of the solution after 11 h of electrolysis at 1.2 V (versus Ag/AgCl) indicated only about 8 % decrease in the catalyst concentration; this is expected owing to the deposition of cobalt complex on the working electrode surface (Figure S13). Hence, the catalyst is still present after a long period of electrolysis. Moreover, the catalyst displayed a linear dependence of catalytic current on the catalyst concentration (Figure S14). This dependence is unlikely to be caused by a surface-adsorbed species because similar catalysis is observed with three different electrode materials (GC, HOPG, and ITO). Furthermore, the in situ generated cobalt complex discloses a catalytic current dependence on the electronic structure of the complex. Thus, the use of the electron-deficient bidentate ligand 1-phenyl triazole-4-carboxylic acid leads to a decrease in the catalytic current of more than 50 % and an increase of the WO overpotential compared with the use of TCA (Figure S15). Llobet and co-workers very recently reported similar findings in their mononuclear copper-based WOC, with which they demonstrated that, as the electron-donating capacity at the aromatic ring increased, the overpotential was drastically reduced.[35]

The apparent catalytic currents for WO prompted us to examine CPE catalyzed by the in situ generated complex $Co(TCA)_2$·$2H_2O$. The experiment was performed at a fixed potential (1.2 V versus Ag/AgCl) in 0.1 M acetate electrolyte (pH 6.0) containing 1 mM of catalyst. The system had a very stable oxygen evolution current density of about 2.0 mA cm^{-2}, and a transparent brown film was observed on ITO after 2 h of electrolysis (Figure S16). The electrocatalyst remains very active during extended periods of CPE over 11 h with a high current density for oxygen evolution (Figure 8). During electrolysis, gas bubbles were clearly observed, and these bubbles were confirmed as oxygen molecules by GC. No apparent O_2 evolution current was observed on the bare ITO immersed in catalyst-free acetate buffer. After 11 h of CBE, the electrode was transferred to a catalyst-free acetate electrolyte of pH ≈ 7.5 to show a stable current density of 2.7 mA cm^{-2} (Figure 8, inset).

Photochemical WO

The catalytic efficiency of the in situ generated complex $Co(TCA)(OH_2)_2$ for visible-light-driven WO was studied by using
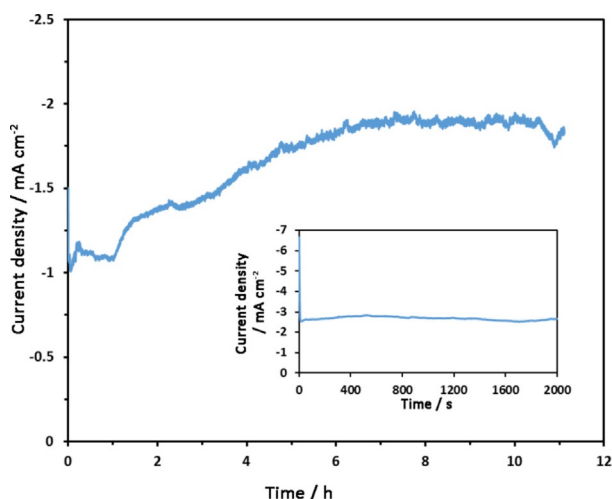
Figure 8. Long-term CPE of ITO electrode in 0.1 M acetate (pH 6.0) containing 1 mM Co−TCA at 1.2 V (versus Ag/AgCl). The inset shows CBE results with the deposited film on the ITO surface in catalyst-free acetate solution at pH 7.5.

[Ru(bpy)$_3$]Cl$_2$ as the PS and Na$_2$S$_2$O$_8$ as the sacrificial oxidant, in a solution of sodium acetate (pH 7.0) under visible-light irradiation ($\lambda > 420$ nm; Figure 9). Oxygen evolution was monitored by using GC with a thermal conductivity detector (TCD). Under photocatalysis, oxygen evolution starts and throughout the first hour the amount of O$_2$ increases linearly to reach about 90 μmol oxygen in the gaseous phase after 1 h of photocatalysis; this corresponds to a turnover number (TON) of 90 (mol of O$_2$ per mol of **1**). Oxygen production stops around 1 h after the start of photoirradiation owing to [Ru(bpy)$_3$]$^{2+}$ degradation, as indicated by a partial decrease of the absorption band at $\lambda = 450$ nm (Figure S17).

Determination of the complex stability for WO under operating conditions such as aqueous medium, pH, and oxidation potential is the first step in proving the molecular nature of the catalytic system. Subsequently, catalyst speciation or isolation and ex situ characterization, where possible, could give
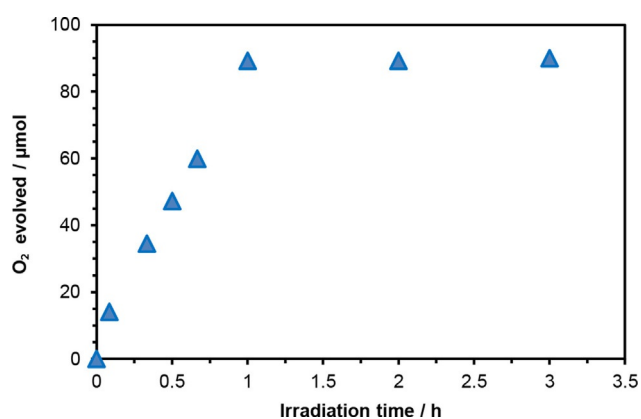
Figure 9. Plot of oxygen evolution versus time for visible-light-driven ($\lambda > 420$ nm) WO catalyzed by Co(TCA)(OH$_2$)$_2$ (100 μM) in aqueous acetate solution (0.1 M, 10 mL; pH 7.5) containing Na$_2$S$_2$O$_8$ (10 mM) and [Ru(bpy)$_3$]Cl$_2$ (1 mM) under N$_2$.

further breakthroughs about the active species during reaction. The molecular identity of the cobalt catalyst (**1**) was proven based on both in situ and ex situ catalyst characterization. First, a solution containing the in situ generated complex Co(TCA)(OH$_2$)$_2$ (0.05 mM), [Ru(bpy)$_3$]Cl$_2$ (10 equiv), and Na$_2$S$_2$O$_8$ (20 equiv) in a solution of acetate (pH 7.5) was subjected to ESI-MS and after 3 h of photoirradiation the solution was analyzed again by means of ESI-MS. The mass spectrum of the photoirradiated sample confirmed the exact molecular weight of the catalyst in solution at m/z 553.41 [Co(TCA)(OH$_2$)$_2$−2 H$^+$], which was the same as that before photocatalysis. This means that the catalyst is very stable under the photocatalysis conditions because it maintains its structure for long periods of photocatalysis (Figure S18). No signal for free dissociated ligand was observed in the ESI-MS spectrum after photocatalysis, which would otherwise appear as at m/z 231, corresponding to TCA. Additionally, no signals from cobalt aqua ions were detected.

Moreover, time-dependent DLS was used to rule out the formation of any cobalt species nanoparticles under photolytic conditions, above the limit of detection, whereas those catalyzed by cobalt acetate did produce particles that were presumably cobalt oxide. Several samples of the photoirradiated catalyst solution were collected at different time intervals (up to 2 h) and no nanoparticles could be detected (Figures S19 and S20).

In situ ESI-MS characterization of the reaction solution before and after the photochemical WO reaction suggested the high stability of the cobalt catalyst and DLS analysis ruled out the formation of nanoparticles during the process. A second and conclusive step in distinguishing homo- and heterogeneous catalysis is isolation of the catalyst and ex situ characterization of any detected forms of the catalyst. Therefore, first, a solution containing 0.1 mM of catalyst **1**, 1 mM of [Ru(bpy)$_3$]Cl$_2$, and 10 mM of Na$_2$S$_2$O$_8$ in acetate buffer (0.1 M) at pH 7.5 was irradiated under visible light for 2 h. After water evaporation at room temperature, the reaction residue was dissolved in chloroform. Providentially, both TCA ligand and cobalt complex Co(TCA)$_2$·2 H$_2$O are soluble in chloroform, as independently tested. The solution in chloroform was then analyzed by ESI-MS and ^{1}H NMR and FTIR spectroscopy. ESI-MS analysis of the post-photocatalysis isolated product revealed an identical mass spectrum to that of the as-synthesized complex, with the absence of any signals corresponding to the free ligand (Figure 10).

The ^{1}H NMR spectrum of the free TCA ligand revealed two sharp signals in the aliphatic region at $\delta = 2.00$ in Figure 10 and 2.39 ppm, which were equivalent to 6 H and 3 H, respectively, from the three methyl groups on the mesityl moiety. After coordination, in the as-synthesized cobalt complex Co(TCA)$_2$·2 H$_2$O, these two signals have clearly shifted to the right with an exchange of their positions. Thus, in the complex, the two signals appeared at $\delta = 1.99$ (equivalent to 3 H) and 2.11 ppm (equivalent to 6 H), whereas the signals in the aromatic region, which were localized close to the cobalt ion, were not well defined because the complex contained the paramagnetic Co^{II} ion. Similarly, the signals of the product iso-
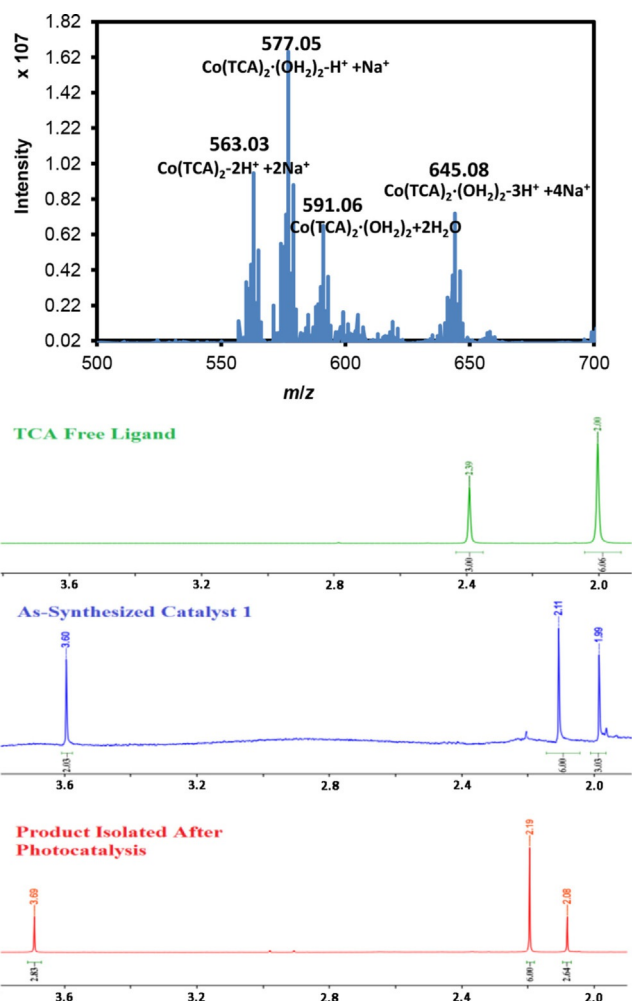
Figure 10. Characterization of the product isolated after 2 h of photoirradiation. Conditions: $Co(TCA)(OH_2)_2$ (0.1 mM), 10 equiv of $[Ru(bpy)_3]Cl_2$ and 100 equiv of $Na_2S_2O_8$ in an acetate solution (pH 7.5) was photoirradiated with a Xe lamp at $\lambda > 420$ nm for 2 h. Top: ESI-MS spectrum. Bottom: ^1H NMR spectra for the comparison of free TCA ligand (green), as-synthesized catalyst (blue), and the isolated product after photocatalysis (red).

DFT calculations

For WO, an electrochemical potential of 1.23 eV per electron is required at pH 0.[36] Some possible catalytic cycles were modeled (Figure 11) and compared with the calculated performance of our complex with other possible WOCs in a volcano plot (Figure 12, see below).

To elucidate the potential WO mechanism, DFT calculations were performed (see the Supporting Information for more de-
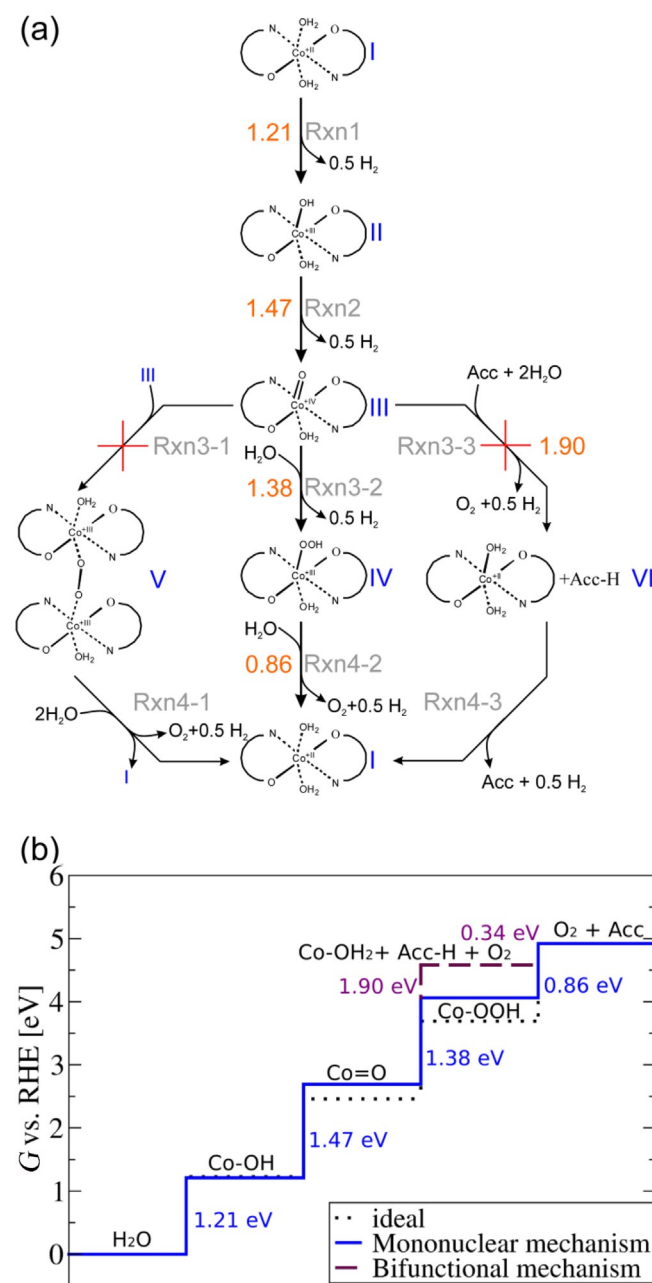
Figure 11. a) WO mechanism pathways. From complex **III**, there are three different possible mechanisms: 1) a binuclear mechanism (through Rxn3-1 and Rxn4-1), 2) a mononuclear mechanism (through Rxn3-2 and Rxn4-2), and 3) a bifunctional mechanism (through Rxn3-3 and Rxn4-3) in which an acceptor (Acc) has a cocatalytic role. b) Stepwise representation of the WO according to the mononuclear mechanism (following Rxn1, Rxn2, Rxn3-2, and Rxn4-2).

lated after photoirradiation are analogous to those of the as-synthesized catalyst (Figure 10). The absence of any signals from the dissociated ligand or its oxidation products, along with retention of the integration ratio of the two signals corresponding to the methyl groups—the same as those in the as-synthesized catalyst—strongly support that the catalyst preserves its molecular identity under photocatalysis conditions. The ^1H NMR spectrum of the post-photocatalysis product noticeably exhibited sharp resonances, with slight changes in chemical shifts that might be a result of oxidation of the complex to the diamagnetic Co^{III} analogue. The ligand oxidation products can be easily detected in ^1H NMR spectroscopy; nonetheless, ^1H NMR spectroscopy did not detect any ligand dissociation or its oxidation products. Also, during photochemical WO, MS could not detect any CO_2 gas; this excludes ligand decomposition under harsh photocatalysis conditions.

tails about the level of theory used). The mechanisms were studied by considering only key intermediates reached through PCETs. The redox potentials were computed by taking advantage of the theoretical NHE developed by Rossmeisl et al.[37] For convenience, we discuss our results with respect to the reversible hydrogen electrode (RHE), which adds a pH correction of 59 meV per pH unit. Accordingly all redox potentials discussed here become pH-independent. In Figure 11 a, the three most common potential water oxidation mechanisms are shown. The first two reaction steps (Figure 11 a, Rxn1 and Rxn2) comprise the subsequent abstraction of H^+/e^- couples, resulting in the formation of Co^{III}—OH hydroxo and Co^{IV}=O oxo intermediates. In the present set of calculations, we find that potentials of 1.21 and 1.47 eV are required for these oxidations steps (versus RHE). The Co^{IV}=O species (**III** in Figure 11 a) corresponds to a branching point from which O—O bond formation can proceed through a variety of different mechanisms. The most common reaction paths summarized in the literature are the binuclear path[38] (Figure 11 a, Rxn3-1), the mononuclear path[37,39] (Figure 11 a, Rxn3-2), and the recently discovered bifunctional path[40] (Figure 11 a, Rxn3-3). Each of the three mechanisms is characterized by different structural requirements. The binuclear mechanism requires the presence of two easily available adjacent cobalt sites to proceed.[41] Due to the mononuclear nature of the complex, the only possibility to fulfill this requirement is the cooperative interaction between two preoxidized complexes, resulting in the formation of a Co—O—O—Co peroxo bridge between them. The rather large π–π-stacking distance of 5–6 Å, however, renders this possibility unlikely. Despite this unfavorable steric hindrance, it is still not impossible to form such a bridge, at the cost of a considerable activation barrier. However, the fact that the complex still displays considerable current density, even after being placed on an ITO electrode upon which freely moving Co=O moieties are no longer available prompts us to exclude this mechanism.

This renders the nucleophilic attack of a water or OH^- molecule the most likely path to O—O bond formation (Figure 11 a, Rxn3-2 and Rxn4-2). Assuming this path, the nucleophilic attack of water is generally assumed to result in the formation of a Co^{III}—OOH intermediate under abstraction of a H^+/e^- couple (Figure 11 a, Rxn3-2).[37,42] Following this mechanism, a potential of 1.38 eV is required for O—O bond formation followed by the release of O_2, which requires a potential of 0.86 eV. Thus, the oxidation of Co—OH to Co=O appears, with an overpotential of 0.24 eV, to be potential determining (Figure 11 b).

Recently, a bifunctional mechanism for the nucleophilic O—O bond-formation step has also been proposed in the heterogeneous electrochemistry community (Figure 11 a, Rxn3-3).[41] In contrast to the classical mononuclear mechanism, O—O bond formation is assumed to occur here in a concerted reaction step, comprising the nucleophilic attack of a water molecule, the abstraction of the H^+/e^- couple, and the transfer of the second hydrogen to an adjacent hydrogen Acc unit (Figure 11 a). This mechanism allows for the direct formation of O_2 and avoids the formation of Co—OOH [Rxn3-3 in Figure 11 a].

$$Co=O + 2 H_2O + Acc \rightarrow [Co-H_2O + Acc-H] + O_2 + 0.5 H_2$$
$$(Rxn3-3)$$
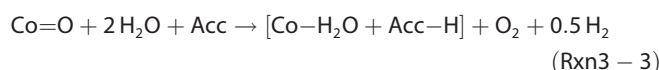
A prerequisite for this mechanism is, however, the availability of a reasonably reactive hydrogen acceptor in close vicinity to the active site. In the present complex, only a nitrogen atom in the triazole ring or a second Co=O could act as a cocatalyst. The former can be excluded because the triazole ring has a redox potential of 0.34 eV versus RHE, rendering it a poor hydrogen acceptor. Indeed, O—O bond formation would, with a redox potential of 1.90 eV versus RHE, become the potential-determining step. Similarly, also hydrogen transfer to Co=O, provided it is accessible under the reaction conditions, would not change the energy landscape because this would not avoid the potential-determining reaction step (Figure 11 a, Rxn2). Additionally, it would add an equally unfavorable reaction step (Figure 11 a, Rxn4-3) for the recovery of the Co=O acceptor unit. Thus, the bifunctional mechanism can be excluded for the present system.

Based on the energetics of the key intermediates, a comparison of the activity of the catalyst with state-of-the-art molecular and solid-state WOCs can be performed by using a volcano plot.[39,43] Volcano plots are drawn by plotting the activity (here the overpotential, η) on the y axis and a descriptor for the activity (here Rxn2 in Figure 11 a) on the x axis. The plot is a graphical representation of Sabatier's principle, which states that for the best possible catalyst all reaction steps display comparable energetics.[44] These ideal catalysts are found at the top of the volcano, whereas less ideal materials are shifted away from the top and appear either on the left branch of the volcano, if the intermediates are bound too strongly, or at the right branch, if they are too unstable. Details on the construction and interpretation of volcano plots can be found in the literature[43a,b] and the Supporting Information.

Let us begin the discussion of the volcano plot shown in Figure 12 by considering the general shape of the oxygen evo-
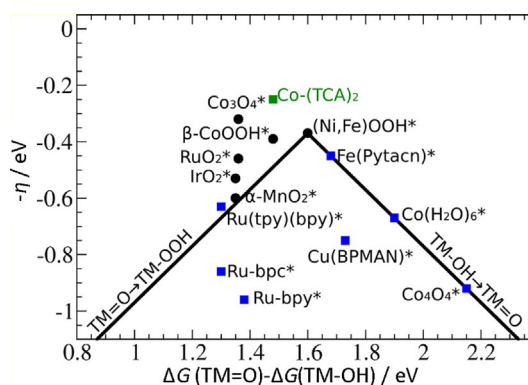
Figure 12. A DFT-based volcano plot relating the theoretical limiting overpotential of various TM complexes and oxide surfaces to general oxygen reduction reaction reactivity trends. RuO_2, IrO_2, Co_3O_4 (Ref. [39]); α-MnO_2 (Ref. [45]); β-CoOOH (Ref. [46]); (Ni,Fe)OOH (Ref. [47]); [Co(H₂O)₆] (Ref. [48]); Co_4O_4 cubane (Ref. [49]); [Fe(Pytacn)] (Pytacn = 1-[2′-(pyridyl)methyl]-4,7-dialkyl-1,4,7-triazacyclononane; Ref. [50]); [Ru(tpy)(bpy)] (tpy = 2,2′;6′,2″-terpyridine; Ref. [51]); [Cu₂(BPMAN)] (BPMAN = 2,7-[bis(2-pyridylmethyl)aminomethyl]-1,8-naphthyridine; Ref. [52]); [Ru(bpc)] and [Ru(bpy)] (Ref. [42]); [Co(TCA)₂] (this work).

lution reaction volcano. The most prominent feature is the peak of the volcano, which is placed at a reaction free energy of 1.6 eV for Rxn2 (Figure 11 a), rather than the thermodynamic potential of 1.23 eV. This is a direct result of the constant energy difference of 3.2 eV observed for a large number of very different systems, ranging from TM oxides to TM-doped graphenes.[39,41b,53] With a theoretical overpotential of only 0.24 eV and a free energy of 1.47 eV for Rxn2 (Figure 11 a), our catalyst falls close to the top of the volcano, slightly shifted to the left branch of the volcano at which point catalysts with intermediates that are too stable are placed. This resembles the excellent performance of the complex observed experimentally. To which extent minor improvements through destabilization of the intermediates with less-electron-donating ligands can be achieved is unclear considering the computational uncertainties associated with the modeling of TM complexes.[54] Furthermore, it is equally active as state-of-the-art dimensionally stable anodes (DSAs) used in industrial WO, which rely on IrO_2 and RuO_2,[39,55] and outperforms many of the recently discovered homogeneous WOCs based on abundant TM oxides.[39,42,46–52,56]

Conclusions

We have demonstrated that the in situ generated $Co(TCA)_2 \cdot 2H_2O$ (TCA = 1-mesityl-1,2,3-1H-triazole-4-carboxylate) is an active catalyst for both the photo- and electrochemical water oxidation (WO) reactions. In electrochemical investigations, the catalyst was found to self-assemble into a catalyst film on the surface of different electrodes, such as glassy carbon (GC), highly oriented pyrolytic graphite (HOPG), and indium-doped tin oxide (ITO) electrodes. The film was proved not to be cobalt oxide/hydroxide, as normally expected, but, for the first time, was a molecular cobalt complex that incorporated the original ligand ligated to cobalt. The film was evidenced based on SEM, Raman, FTIR, and X-Ray photoelectron spectroscopy (XPS) results, along with its physical properties. Similar results were observed with the copper(II)/6,6-dihydroxy-2,2-bipyridine catalytic system when used for electrochemical WO, during which a deposit was observed on the electrode during electrolysis experiments and it was demonstrated that this film was oligo- or polymers of the copper complex instead of copper oxide.[24] Moreover, in the photochemical WO, the catalytic activity of the complex competes with some of the best water oxidation catalysts (WOCs) reported so far in terms of stability and turnover number (TON). The molecular identity of the catalyst in the photocatalysis process was evidenced based on ESI-MS, dynamic light scattering (DLS), FTIR, and ^1H NMR spectroscopic characterization. Proof of the high stability of the in situ generated complex and its high catalytic activity under neutral conditions, based only on a bidentate ligand, shed light on the ability of small ligands, instead of presynthesized polydentate ligands, to stabilize cobalt ions in lower and higher oxidation states. Furthermore, DFT calculations predicted a mononuclear oxidation mechanism and showed that this $Co(TCA)_2 \cdot 2H_2O$ catalyst lay very close to the top of the theoretical volcano plot. Based on these compu-

tational results, we are confident that small modifications of this type of catalyst can lead to a superb, easily synthesized, industrial WOC.

Acknowledgements

[1] Y. Umena, K. Kawakami, J.-R. Shen, N. Kamiya, *Nature* **2011**, *473*, 55–60.

[2] a) M. D. Kärkäs, O. Verho, E. V. Johnston, B. R. Åkermark, *Chem. Rev.* **2014**, *114*, 11863–12001; b) J. D. Blakemore, R. H. Crabtree, G. W. Brudvig, *Chem. Rev.* **2015**, *115*, 12974–13005.

[3] a) L. Duan, Y. Xu, L. Tong, L. Sun, *ChemSusChem* **2011**, *4*, 238–244; b) D. G. Hetterscheid, J. N. Reek, *Angew. Chem. Int. Ed.* **2012**, *51*, 9740–9747; *Angew. Chem.* **2012**, *124*, 9878–9885; c) N. Kaveevivitchai, R. Zong, H.-W. Tseng, R. Chitta, R. P. Thummel, *Inorg. Chem.* **2012**, *51*, 2930–2939; d) L. Tong, A. K. Inge, L. Duan, L. Wang, X. Zou, L. Sun, *Inorg. Chem.* **2013**, *52*, 2505–2518; e) L. Tong, Y. Wang, L. Duan, Y. Xu, X. Cheng, A. Fischer, M. R. S. Ahlquist, L. Sun, *Inorg. Chem.* **2012**, *51*, 3388–3398; f) A. G. Walden, A. J. Miller, *Chem. Sci.* **2015**, *6*, 2405–2410; g) C. Wang, Y. Chen, W.-F. Fu, *Dalton Trans.* **2015**, *44*, 14483–14493; h) Q. Zeng, F. W. Lewis, L. M. Harwood, F. Hartl, *Coord. Chem. Rev.* **2015**, *304*, 88–101; lit i> W. Su, H. A. Younus, K. Zhou, Z. A. K. Khattak, S. Chaemcheun, C. Chen, F. Verpoort, *Catal. Sci. Technol.* **2017**, *7*, 387-395.

[4] a) A. Lewandowska-Andralojc, D. E. Polyansky, C.-H. Wang, W.-H. Wang, Y. Himeda, E. Fujita, *Phys. Chem. Chem. Phys.* **2014**, *16*, 11976–11987; b) N. D. McDaniel, F. J. Coughlin, L. L. Tinker, S. Bernhard, *J. Am. Chem. Soc.* **2008**, *130*, 210–217; c) J. A. Woods, R. Lalrempuia, A. Petronilho, N. D. McDaniel, H. Müller-Bunz, M. Albrecht, S. Bernhard, *Energy Environ. Sci.* **2014**, *7*, 2316–2328; d) M. Li, K. Takada, J. I. Goldsmith, S. Bernhard, *Inorg. Chem.* **2016**, *55*, 518–526; e) M. Navarro, M. Li, H. Müller-Bunz, S. Bernhard, M. Albrecht, *Chem. Eur. J.* **2016**, *22*, 6740–6745.

[5] a) M. A. Asraf, H. A. Younus, C. I. Ezugwua, A. Mehta, *Catal. Sci. Technol.* **2016**, *6*, 4271–4282; b) M. A. Asraf, H. A. Younus, M. Yusubov, F. Verpoort, *Catal. Sci. Technol.* **2015**, *5*, 4901–4925; c) C. Lu, J. Du, X.-J. Su, M.-T. Zhang, X. Xu, T. J. Meyer, Z. Chen, *ACS Catal.* **2016**, *6*, 77–83; d) Y. Zhao, J. Lin, Y. Liu, B. Ma, Y. Ding, M. Chen, *Chem. Commun.* **2015**, *51*, 17309–17312; e) D. Das, S. Pattanayak, K. K. Singh, B. Garai, S. Sen Gupta, *Chem. Commun.* **2016**, *52*, 11787–11790.

[6] a) S. M. Barnett, K. I. Goldberg, J. M. Mayer, *Nat. Chem.* **2012**, *4*, 498–502; b) Z. Chen, T. J. Meyer, *Angew. Chem. Int. Ed.* **2013**, *52*, 700–703; *Angew. Chem.* **2013**, *125*, 728–731; c) M.-T. Zhang, Z. Chen, P. Kang, T. J. Meyer, *J. Am. Chem. Soc.* **2013**, *135*, 2048–2051.

[7] a) W. A. Arafa, M. D. Kärkäs, B.-L. Lee, T. Åkermark, R.-Z. Liao, H.-M. Berends, J. Messinger, P. E. Siegbahn, B. Åkermark, *Phys. Chem. Chem. Phys.* **2014**, *16*, 11950–11964; b) E. A. Karlsson, B. L. Lee, R. Z. Liao, T. Åkermark, M. D. Kärkäs, V. S. Becerril, P. E. Siegbahn, X. Zou, M. Abrahamsson, B. Åkermark, *ChemPlusChem* **2014**, *79*, 936–950.

[8] a) B. Das, B.-L. Lee, E. A. Karlsson, T. Åkermark, A. Shatskiy, S. Demeshko, R.-Z. Liao, T. M. Laine, M. Haukka, E. Zeglio, A. F. Abdel-Magied, P. E. M. Siegbahn, F. Meyer, M. D. Karkas, E. V. Johnston, E. Nordlander, B. Åkermark, *Dalton Trans.* **2016**, *45*, 13289–13293; b) W. C. Ellis, N. D. McDaniel, S. Bernhard, T. J. Collins, *J. Am. Chem. Soc.* **2010**, *132*, 10990–10991; c) J. L. Fillol, Z. Codolà, I. Garcia-Bosch, L. Gómez, J. J. Pla, M. Costas, *Nat. Chem.* **2011**, *3*, 807–813; d) B. M. Klepser, B. M. Bartlett, *J.*

Am. Chem. Soc. **2014**, *136*, 1694–1697; e) B. Das, A. Orthaber, S. Ott, A. Thapper, *ChemSusChem* **2016**, *9*, 1178–1186; f) G. Panchbhai, W. M. Singh, B. Das, R. T. Jane, A. Thapper, *Eur. J. Inorg. Chem.* **2016**, 3262–3268; g) C. Panda, J. Debgupta, D. D. Díaz, K. K. Singh, G. S. Sen, B. B. Dhar, *J. Am. Chem. Soc.* **2014**, *136*, 12273–12282; h) Y. Liu, R. Xiang, X. Du, Y. Ding, B. Ma, *Chem. Commun.* **2014**, *50*, 12779–12782.

[9] a) D. Wang, G. Ghirlanda, J. P. Allen, *J. Am. Chem. Soc.* **2014**, *136*, 10198–10201; b) L. Wang, L. Duan, R. B. Ambre, Q. Daniel, H. Chen, J. Sun, B. Das, A. Thapper, J. Uhlig, P. Dinér, *J. Catal.* **2016**, *335*, 72–78; c) Y. Han, Y. Wu, W. Lai, R. Cao, *Inorg. Chem.* **2015**, *54*, 5604–5613.

[10] a) J. Suntivich, K. J. May, H. A. Gasteiger, J. B. Goodenough, Y. Shao-Horn, *Science* **2011**, *334*, 1383–1385; b) Z. Zhuang, W. Sheng, Y. Yan, *Adv. Mater.* **2014**, *26*, 3950–3955; c) R. D. Smith, M. S. Prévot, R. D. Fagan, Z. Zhang, P. A. Sedach, M. K. J. Siu, S. Trudel, C. P. Berlinguette, *Science* **2013**, *340*, 60–63; d) J. Masa, W. Xia, I. Sinev, A. Zhao, Z. Sun, S. Grützke, P. Weide, M. Muhler, W. Schuhmann, *Angew. Chem. Int. Ed.* **2014**, *53*, 8508–8512; *Angew. Chem.* **2014**, *126*, 8648–8652; e) L.-A. Stern, L. Feng, F. Song, X. Hu, *Energy Environ. Sci.* **2015**, *8*, 2347–2351.

[11] a) M. W. Kanan, D. G. Nocera, *Science* **2008**, *321*, 1072–1075; b) D. Wang, J. T. Groves, *Proc. Natl. Acad. Sci. USA* **2013**, *110*, 15579–15584; c) P. Du, R. Eisenberg, *Energy Environ. Sci.* **2012**, *5*, 6012–6021; d) Z. Chen, T. J. Meyer, *Angew. Chem. Int. Ed.* **2013**, *52*, 13708–13711; *Angew. Chem.* **2013**, *125*, 13953–13956; e) M. Dincă, Y. Surendranath, D. G. Nocera, *Proc. Natl. Acad. Sci. USA* **2010**, *107*, 10337–10341; f) A. K. Poulsen, A. Rompel, C. J. McKenzie, *Angew. Chem. Int. Ed.* **2005**, *44*, 6916–6920; *Angew. Chem.* **2005**, *117*, 7076–7080; g) R. K. Hocking, R. Brimblecombe, L.-Y. Chang, A. Singh, M. H. Cheah, C. Glover, W. H. Casey, L. Spiccia, *Nat. Chem.* **2011**, *3*, 461–466; h) E. A. Karlsson, B.-L. Lee, T. Åkermark, E. V. Johnston, M. D. Kärkäs, J. Sun, Ö. Hansson, J.-E. Bäckvall, B. Åkermark, *Angew. Chem. Int. Ed.* **2011**, *50*, 11715–11718; *Angew. Chem.* **2011**, *123*, 11919–11922; i) M. Zhang, M.-T. Zhang, C. Hou, Z.-F. Ke, T.-B. Lu, *Angew. Chem. Int. Ed.* **2014**, *53*, 13042–13048; *Angew. Chem.* **2014**, *126*, 13258–13264; j) M. M. Najafpour, G. Renger, M. Hołyńska, A. N. Moghaddam, E.-M. Aro, R. Carpentier, H. Nishihara, J. J. Eaton-Rye, J.-R. Shen, S. I. Allakhverdiev, *Chem. Rev.* **2016**, *116*, 2886–2936; k) S. D. Tilley, M. Cornuz, K. Sivula, M. Grätzel, *Angew. Chem. Int. Ed.* **2010**, *49*, 6405; *Angew. Chem.* **2010**, *122*, 6549; l) M. D. Kärkäs, B. Åkermark, *Dalton Trans.* **2016**, *45*, 14421; m) K. S. Joya, Y. F. Joya, H. J. De Groot, *Adv. Energy Mater.* **2014**, *4*, 1301929.

[12] a) V. Artero, M. Chavarot-Kerlidou, M. Fontecave, *Angew. Chem. Int. Ed.* **2011**, *50*, 7238–7266; *Angew. Chem.* **2011**, *123*, 7376–7405; b) C.-F. Leung, S.-M. Ng, C.-C. Ko, W.-L. Man, J. Wu, L. Chen, T.-C. Lau, *Energy Environ. Sci.* **2012**, *5*, 7903–7907; c) B. M. Hunter, H. B. Gray, A. M. Müller, *Chem. Rev.* **2016**, *116*, 14120.

[13] a) J. J. Stracke, R. G. Finke, *ACS Catal.* **2014**, *4*, 909–933; b) J. J. Stracke, R. G. Finke, *J. Am. Chem. Soc.* **2011**, *133*, 14872–14875.

[14] V. Artero, M. Fontecave, *Chem. Soc. Rev.* **2013**, *42*, 2338–2356.

[15] a) Q. Yin, J. M. Tan, C. Besson, Y. V. Geletii, D. G. Musaev, A. E. Kuznetsov, Z. Luo, K. I. Hardcastle, C. L. Hill, *Science* **2010**, *328*, 342–345; b) H. Y. Wang, E. Mijangos, S. Ott, A. Thapper, *Angew. Chem. Int. Ed.* **2014**, *53*, 14499; *Angew. Chem.* **2014**, *126*, 14727; c) J.-W. Wang, P. Sahoo, T.-B. Lu, *ACS Catal.* **2016**, *6*, 5062–5068.

[16] A. M. Ullman, Y. Liu, M. Huynh, D. K. Bediako, H. Wang, B. L. Anderson, D. C. Powers, J. J. Breen, H. D. Abruña, D. G. Nocera, *J. Am. Chem. Soc.* **2014**, *136*, 17681–17688.

[17] a) T. Abe, K. Nagai, S. Kabutomori, M. Kaneko, A. Tajiri, T. Norimatsu, *Angew. Chem. Int. Ed.* **2006**, *45*, 2778–2781; *Angew. Chem.* **2006**, *118*, 2844–2847; b) D. K. Dogutan, R. McGuire, Jr, D. G. Nocera, *J. Am. Chem. Soc.* **2011**, *133*, 9178–9180; c) T. Nakazono, A. R. Parent, K. Sakai, *Chem. Commun.* **2013**, *49*, 6325–6327; d) E. Pizzolato, M. Natali, B. Posocco, A. M. López, I. Bazzan, M. Di Valentin, P. Galloni, V. Conte, M. Bonchio, F. Scandola, *Chem. Commun.* **2013**, *49*, 9941–9943; e) D. J. Wasylenko, C. Ganesamoorthy, J. Borau-Garcia, C. P. Berlinguette, *Chem. Commun.* **2011**, *47*, 4249–4251; f) M. L. Rigsby, S. Mandal, W. Nam, L. C. Spencer, A. Llobet, S. S. Stahl, *Chem. Sci.* **2012**, *3*, 3058–3062; g) Z. Huang, Z. Luo, Y. V. Geletii, J. W. Vickers, Q. Yin, D. Wu, Y. Hou, Y. Ding, J. Song, D. G. Musaev, C. L. Hill, T. Lian, *J. Am. Chem. Soc.* **2011**, *133*, 2068–2071; h) H. Lv, J. Song, Y. V. Geletii, J. W. Vickers, J. M. Sumliner, D. G. Musaev, P. Kögerler, P. F. Zhuk, J. Bacsa, G. Zhu, C. L. Hill, *J. Am. Chem. Soc.* **2014**, *136*, 9268–9271; i) Y. V. Geletii, B. Botar, P. Kögerler, D. A. Hillesheim, D. G. Musaev, C. L. Hill, *Angew. Chem. Int. Ed.* **2008**, *47*, 3896–3899;

[18] a) L. Duan, F. Bozoglian, S. Mandal, B. Stewart, T. Privalov, A. Llobet, L. Sun, *Nat. Chem.* **2012**, *4*, 418–423; b) L. Duan, L. Wang, F. Li, F. Li, L. Sun, *Acc. Chem. Res.* **2015**, *48*, 2084–2096.

[19] a) L. Tong, M. Gothelid, L. Sun, *Chem. Commun.* **2012**, *48*, 10025–10027; b) Y. Chen, H. Chen, H. Tian, *Chem. Commun.* **2015**, *51*, 11508–11511.

[20] S. Dey, B. Mondal, A. Dey, *Phys. Chem. Chem. Phys.* **2014**, *16*, 12221–12227.

[21] A. Han, H. Wu, Z. Sun, H. Jia, Z. Yan, H. Ma, X. Liu, P. Du, *ACS Appl. Mater. Interfaces* **2014**, *6*, 10929–10934.

[22] K. S. Joya, K. Takanabe, H. J. De Groot, *Adv. Energy Mater.* **2014**, *4*, 1400252.

[23] D. Hong, J. Jung, J. Park, Y. Yamada, T. Suenobu, Y.-M. Lee, W. Nam, S. Fukuzumi, *Energy Environ. Sci.* **2012**, *5*, 7606–7616.

[24] T. Zhang, C. Wang, S. Liu, J.-L. Wang, W. Lin, *J. Am. Chem. Soc.* **2014**, *136*, 273–281.

[25] K. S. Joya, N. K. Subbaiyan, F. D'Souza, H. J. de Groot, *Angew. Chem. Int. Ed.* **2012**, *51*, 9601–9605; *Angew. Chem.* **2012**, *124*, 9739–9743.

[26] B. S. Yeo, A. T. Bell, *J. Am. Chem. Soc.* **2011**, *133*, 5587–5593.

[27] D. Ressnig, M. Shalom, J. Patscheider, R. Moré, F. Evangelisti, M. Antonietti, G. R. Patzke, *J. Mater. Chem. A* **2015**, *3*, 5072–5082.

[28] J-W Wang, P. Sahoo, T-B Lu, *ACS Catal.* **2016**, *6*, 5062–5068.

[29] J. J. Goldstein, D. E. Newbury, P. Echlin, D. C. Joy, A. D. Romig, Jr, C. E. Lyman, C. Fiori, E. Lifshin, *Scanning Electron Microscopy and X-ray Microanalysis: A Text for Biologists, Materials Scientists, and Geologists*, Springer, Berlin, **2012**.

[30] a) N. S. McIntyre, M. G. Cook, *Anal. Chem.* **1975**, *47*, 2208–2213; b) C. A. Kent, J. J. Concepcion, C. J. Dares, D. A. Torelli, A. J. Rieth, A. S. Miller, P. G. Hoertz, T. J. Meyer, *J. Am. Chem. Soc.* **2013**, *135*, 8432–8435; c) F. Song, Y. Ding, B. Ma, C. Wang, Q. Wang, X. Du, S. Fu, J. Song, *Energy Environ. Sci.* **2013**, *6*, 1170–1184; d) J. Matthew, *Surf. Interface Anal.* **2004**, *36*, 1647–1647.

[31] a) S. D. Techane, L. J. Gamble, D. G. Castner, *J. Phys. Chem. C* **2011**, *115*, 9432–9441; b) N. Wu, L. Fu, M. Su, M. Aslam, K. C. Wong, V. P. Dravid, *Nano Lett.* **2004**, *4*, 383–386.

[32] S. C. Petitto, E. M. Marsh, G. A. Carson, M. A. Langell, *J. Mol. Catal. A* **2008**, *281*, 49–58.

[33] S. Ciampi, T. Böcking, K. A. Kilian, M. James, J. B. Harper, J. J. Gooding, *Langmuir* **2007**, *23*, 9320–9329.

[34] R. L. Arechederra, K. Artyushkova, P. Atanassov, S. D. Minteer, *ACS Appl. Mater. Interfaces* **2010**, *2*, 3295–3302.

[35] P. Garrido-Barros, I. Funes-Ardoiz, S. Drouet, J. Bene tBuchholz, F. Maseras, A. Llobet, *J. Am. Chem. Soc.* **2015**, 137, 6758–6761.

[36] *CRC Handbook of Chemistry and Physics, Vol. 85* (Ed.: D. R. Lide), CRC Press, Boca Raton, FL, **2004**.

[37] a) J. Rossmeisl, Z. W. Qu, H. Zhu, G. J. Kroes, J. K. Norskov, *J. Electroanal. Chem.* **2007**, *607*, 83–89; b) J. Rossmeisl, A. Logadottir, J. K. Norskov, *Chem. Phys.* **2005**, *319*, 178–184.

[38] a) J. O. Bockris, T. Otagawa, *J. Phys. Chem-Us* **1983**, *87*, 2960–2971; b) M. Busch, E. Ahlberg, I. Panas, *Phys. Chem. Chem. Phys.* **2011**, *13*, 15069–15076.

[39] I. C. Man, H. Y. Su, F. Calle-Vallejo, H. A. Hansen, J. I. Martinez, N. G. Inoglu, J. Kitchin, T. F. Jaramillo, J. K. Norskov, J. Rossmeisl, *ChemCatChem* **2011**, *3*, 1159–1165.

[40] R. Frydendal, M. Busch, N. B. Halck, E. A. Paoli, P. Krtil, I. Chorkendorff, J. Rossmeisl, *ChemCatChem* **2015**, *7*, 149–154.

[41] a) N. B. Halck, V. Petrykin, P. Krtil, J. Rossmeisl, *Phys. Chem. Chem. Phys.* **2014**, *16*, 13682–13688; b) M. Busch, N. B. Halck, U. I. Kramm, S. Siahrostami, P. Krtil, J. Rossmeisl, *Nano Energy* **2016**, *29*, 126–135.

[42] J. M. de Ruiter, R. L. Purchase, A. Monti, C. J. M. van der Ham, M. P. Gullo, K. S. Joya, M. D'Angelantonio, A. Barbieri, D. G. H. Hetterscheid, H. J. M. de Groot, F. Buda, *ACS Catal.* **2016**, *6*, 7340–7349.

[43] a) M. D. Wodrich, M. Busch, C. Corminboeuf, *Chem. Sci.* **2016**, *7*, 5723–5735; b) M. Busch, M. D. Wodrich, C. Corminboeuf, *Chem. Sci.* **2015**, *6*, 6754–6761; c) R. Parsons, *Trans. Faraday Soc.* **1958**, *54*, 1053–1063; d) J. K. Nørskov, T. Bligaard, J. Rossmeisl, C. H. Christensen, *Nat. Chem.* **2009**, *1*, 37–46; e) H. Gerischer, *Bull. Soc. Chim. Belg.* **1958**, *67*, 506–527.

[44] P. La Sabatier, *Catalyse en Chimie Organique*, Librarie Polytechnique, Paris, **1993**.

[45] M. Lehtimäki, H. Hoffmannová, O. Boytsova, Z. Bastl, M. Busch, N. B. Halck, J. Rossmeisl, P. Krtil, *Electrochim. Acta* **2016**, *191*, 452–461.

[46] M. Bajdich, M. Garcia-Mota, A. Vojvodic, J. K. Norskov, A. T. Bell, *J. Am. Chem. Soc.* **2013**, *135*, 13521–13530.

[47] O. Diaz-Morales, I. Ledezma-Yanez, M. T. M. Koper, F. Calle-Vallejo, *ACS Catal.* **2015**, *5*, 5380–5387.

[48] S. Chu, E. Coccia, M. Barborini, L. Guidoni, *J. Chem. Theory Comput.* **2016**, *12*, 5803.

[49] F. H. Hodel, S. Luber, *ACS Catal.* **2016**, *6*, 1505–1517.

[50] F. Acuña-Parés, Z. Codolà, M. Costas, J. M. Luis, J. Lloret-Fillol, *Chem. Eur. J.* **2014**, *20*, 5696–5707.

[51] D. E. Polyansky, J. T. Muckerman, J. Rochford, R. F. Zong, R. P. Thummel, E. Fujita, *J. Am. Chem. Soc.* **2011**, *133*, 14649–14665.

[52] X. J. Su, M. Gao, L. Jiao, R. Z. Liao, P. E. M. Siegbahn, J. P. Cheng, M. T. Zhang, *Angew. Chem. Int. Ed.* **2015**, *54*, 4909–4914; *Angew. Chem.* **2015**, *127*, 4991–4996.

[53] a) F. Calle-Vallejo, J. I. Martinez, J. M. Garcia-Lastra, E. Abad, M. T. M. Koper, *Surf. Sci.* **2013**, *607*, 47–53; b) M. T. M. Koper, *J. Electroanal. Chem.* **2011**, *660*, 254–260.

[54] C. J. Cramer, D. G. Truhlar, *Phys. Chem. Chem. Phys.* **2009**, *11*, 10757–10816.

[55] S. Trasatti, *Electrochim. Acta* **2000**, *45*, 2377–2385.

[56] D. Friebel, M. W. Louie, M. Bajdich, K. E. Sanwald, Y. Cai, A. M. Wise, M. J. Cheng, D. Sokaras, T. C. Weng, R. Alonso-Mori, R. C. Davis, J. R. Bargar, J. K. Norskov, A. Nilsson, A. T. Bell, *J. Am. Chem. Soc.* **2015**, *137*, 1305–1313.